Pattern Recognition Letters 94 (2017) 62–67

Contents lists available at ScienceDirect

Pattern Recognition Letters

journal homepage: www.elsevier.com/locate/patrec

A hybrid method for underwater image correction

Chongyi Li[a], Jichang Guo[a,*], Chunle Guo[a], Runmin Cong[a], Jiachang Gong[b]

[a] School of Electrical and Information Engineering, Tianjin University, Weijing Road 92, Tianjin and 300300, China
[b] Department of Criminal Science and Technique, China Criminal Police University, Huanggudi Strict Tawan Street 83, Shenyang and 11000, China

ARTICLE INFO

Article history:
Received 26 May 2016
Available online 24 May 2017

Keywords:
Underwater image correction
Color casts
Image degradation
Visibility recovery

ABSTRACT

Underwater images surfer from serious color deviation and blurring due to the effects of light absorption and scattering. In this letter, a hybrid method, which includes color correction and underwater image dehazing, is proposed to improve the visual quality of degraded underwater images. Firstly, an efficient color correction algorithm is applied to remove color casts of underwater images. Then, underwater image dehazing method is proposed to improve the visibility of underwater images, which includes a global background light estimation algorithm specialized for underwater images and a medium transmission estimation algorithm based on the combination a regression model with the characteristics of light traveling in water medium. Since there is no available dataset in this relatively new research area, a dataset which includes 45 underwater images with a wide variety of contents is collected. Subjective and objective performance evaluations demonstrate that the proposed method significantly improves both color and visibility of degraded underwater images, and is comparable to and even outperforms several state-of-the-art methods.

1. Introduction

The visual quality of underwater images plays a crucial role in many ocean engineering applications and scientific researches, such as marine ecological research [28] and ocean rescue [20]. However, underwater images are characterized by low contrast, limited visibility, and diminished color due to the effects of light absorption and scattering. For underwater scenario, light with different wavelengths is absorbed at different rates, which leads to the serious color casts. Moreover, light scattering blurs image features and decreases contrast. Thus, underwater image correction techniques are desired in both scientific researches and computer applications.

In this letter, a hybrid underwater image correction method, which includes color correction and underwater image dehazing, is proposed. Our contributions are four-fold: (1) to our best knowledge, it is the first method that estimates medium transmission of underwater image by combining learning-based strategy with the characteristics of light traveling in water medium; (2) a global background light estimation algorithm specialized for underwater images is proposed based on background light region detection and underwater optical property; (3) an underwater image dataset which includes 45 underwater images with a wide variety of contents collected from the Internet is presented; and (4) the proposed method does not require complex information about the underwater scenes and user interaction.

In the rest of the letter, we give a brief overview of the related work in Section 2. In Section 3, we introduce the color correction method used in this letter. Section 4 describes the proposed underwater image dehazing method. Section 5 presents the experimental results, and Section 6 concludes this letter.

2. Related work

A variety of methods have been proposed to improve the visual quality of degraded underwater images, and can be roughly classified from two aspects: restoration method and enhancement method.

Restoration method regards the recovery of underwater image as an inverse problem, which restores underwater images by estimating parameters of underwater image formation model. Trucco and Olmos-Antillon devised a self-tuning image restoration filter based on a simplified version of underwater image formation model. [30]. Optimal filter parameters are estimated based on a global contrast measure. Carlevaris-Bianco et al. proposed a prior that exploits the strong difference in attenuation among the three color channels of an underwater image to estimate the depth of scene [6]. Chiang and Chen combined a dehazing algorithm with wavelength compensation to restore underwater images [7]. Galdran et al. restored red channel to recover the lost contrast of un-

* Corresponding author.
E-mail addresses: lichongyi@tju.edu.cn (C. Li), jcguo@tju.edu.cn (J. Guo).

http://dx.doi.org/10.1016/j.patrec.2017.05.023
0167-8655/

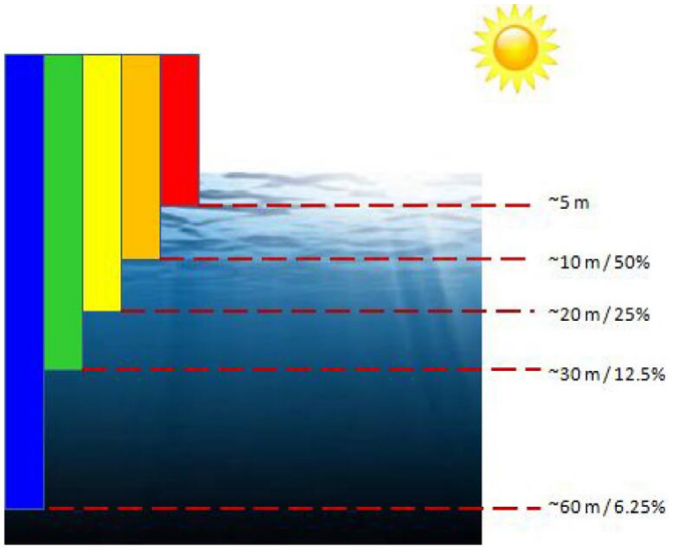

Fig. 1. Different light is attenuated at different rates in water.

derwater images [11]. Peng et al. adopted image blurriness with the image formation model to estimate the distance between the scene point and the camera, and thereby recovered underwater images [25]. Drews et al. extended the classical dark channel prior algorithm [14] to underwater image restoration [9].

Enhancement method does not rely on any image formation model, and enhances underwater images by modifying image pixel values. Iqbal et al. proposed an integrated color model and an unsupervised color correction method to enhance the visual quality of underwater images [17,18]. Ancuti et al. proposed a fusion-based method to increase the contrast of underwater images and videos [1]. Chani and Isa improved contrast and reduced noise of underwater images through modifying the integrated color model [12]. Li and Guo proposed an underwater image enhancement method based on dehazing and color correction [22]. Fu et al. proposed a simple yet effective underwater image color correction algorithm [10]. Bianco et al. proposed a new color correction method for underwater imaging. This method demonstrated the effectiveness of color correction in $L\alpha\beta$ color space [3]. Liu and Chau corrected color cast of underwater images based on surface reflectance statistics [23]. Despite the remarkable progress on underwater image correction methods, it is still an open problem.

3. Color correction

Unlike common images, underwater images usually suffer from more serious color casts (bluish or greenish) due to the special underwater imaging and lighting conditions. As shown in Fig. 1, different light is attenuated at different rates, which leads to color casts of underwater images. Generally, red light disappears at depth of 5 m in water, and then brown light and yellow light disappear, finally green light and blue light disappear at depths of 30 m and 60 m. This is the main reason why most underwater images are dominated by blue-green coloration. Color casts affects the visual quality of underwater images. Therefore, we first remove the color cast and restore underwater images to the relatively genuine color.

Fu et al. proposed a simple yet effective color correction algorithm [10]. In this letter, to remove the effects of color casts, we use this color correction algorithm as our pre-processing based on its effectiveness and low-complexity. Based on extensive statistics, Fu et al. found that the maximum $C(x)^c_{\max}$ and the minimum $C(x)^c_{\min}$ color deviation in each color channel (i.e., RGB) for underwater image can be defined as:

$$C(x)^c_{max} = f(x)^c_m + \eta^c \cdot f(x)^c_v, c \in \{r, g, b\}, \tag{1}$$

$$C(x)^c_{min} = f(x)^c_m - \eta^c \cdot f(x)^c_v, c \in \{r, g, b\}, \tag{2}$$

where $f(x)^c_m$ is the mean value, $f(x)^c_v$ is the mean square error value, and η^c is a parameter, which tempers the saturation of result. Then, color corrected underwater image $f(x)^c_{CR}$ is obtained by:

$$f(x)^c_{CR} = \frac{f(x)^c - C(x)^c_{min}}{C(x)^c_{max} - C(x)^c_{min}} \times 255, c \in \{r, g, b\}, \tag{3}$$

where $f(x)^c$ is input image. Replacing $C(x)^c_{\max}$ and $C(x)^c_{\min}$ with (1) and (2), (3) is translated to:

$$f(x)^c_{CR} = \frac{f(x)^c - f(x)^c_m + \eta^c \cdot f(x)^c_v}{2\eta^c \cdot f(x)^c_v} \times 255. \tag{4}$$

In Fu et al.'s work [10], the saturation parameter η^c is a heuristic value and set to 3 for each color channel. Fig. 2 shows several examples of color corrected results.

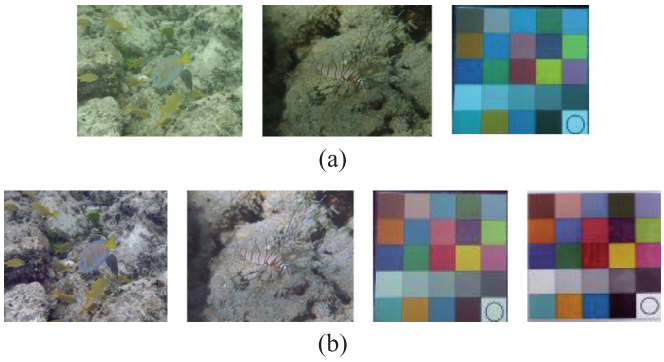

Fig. 2. Color corrected underwater images. (a) Raw underwater images. (b) Color corrected underwater images using the algorithm proposed by [10]. The last image in (b) is the ground truth of color checker image. The raw color checker image and ground truth are obtained from [16].

In Fig. 2, the greenish tone in the raw underwater images (first two images) is removed by the algorithm [10]. For the underwater color checker image, more color details are unveiled in the color corrected image when compared with ground truth. We do not have enough underwater images with ground truth to verify the accuracy and robustness of this color correction algorithm. Nevertheless, after processing by this algorithm, the color of underwater images looks more pleasing and genuine than before, which is desired in our framework.

4. Underwater image dehazing

4.1. Problem formulation

Inspired by classical dark channel prior [14] and learning-based [29] image dehazing methods, our underwater image dehazing method estimates medium transmission of an underwater image based on learning-based strategy and the characteristics of light traveling in water medium. Follow previous work [26] and [7], simplified McGlamery–Jaffe underwater image formation model [24] and [19] is described as:

$$I^c(x) = J^c(x)t^c(x) + A^c(1 - t^c(x)), c \in \{r, g, b\}, \tag{5}$$

where $I^c(x)$ is the degraded underwater image, $J^c(x)$ is the clear underwater image, A^c is the global background light, and $t^c(x)$ is the medium transmission. Furthermore, the medium transmission is expressed as:

$$t^c(x) = \exp(-p^c d(x)), c \in \{r, g, b\}, \tag{6}$$

where $d(x)$ is the distance between the scene point and the camera, p^c is the total attenuation coefficient, which can be decomposed as a linear superposition of absorption coefficient a^c and scattering coefficient b^c. b^c is the superposition of all scattering events at all angles, and is expressed as:

$$b^c = \int_0^{\pi} \beta^c(\omega)\, \mathrm{d}\omega = 2\pi \int_0^{\pi} \beta^c(\theta) \sin\theta\, \mathrm{d}\theta, \tag{7}$$

where $\beta^c(\theta)$ is the integral of the volume scattering function over all solid angles. To obtain $J^c(x)$, we need to estimate global background light A^c, total attenuation coefficient p^c, and medium transmission $t^c(x)$ in the next section.

4.2. Estimating global background light

Global background light A^c is an RGB vector that represents the intensity of the scattered light in the scene at each color channel. In general, the global background light is far away from the camera. We first locate the background light regions of underwater image where global background light might appear. Our experiments found that background light regions usually have the properties of flat and high brightness. The high brightness regions are selected as:

$$Y_b(x) = \begin{cases} 0 & Y(x) < \alpha \\ 1 & Y(x) \geq \alpha. \end{cases} \tag{8}$$

where Y is the light channel (Lab color space), Y_b is the binaryzation of Y, and $\alpha = Y_{mean} + (255 - Y_{mean})/3$ is the threshold which is used to select high brightness regions. $Y_b = 1$ represents high brightness regions. To remove the effects of noise, Gaussian filter is used to smooth the light channel Y. Then, we compute the gradient map G of the light channel Y. The flat regions are selected as:

$$G_b(x) = \begin{cases} 1 & G(x) < \gamma \\ 0 & G(x) \geq \gamma. \end{cases} \tag{9}$$

where G_b is the binaryzation of gradient G, and $\gamma = \min(T_G, \delta)$ is the threshold which is used to select flat regions. Here, T_G is the ceiling gradient value of the gradient histogram distribution with maximum probability. In addition, $\delta = 20$ is a heuristic value. $G_b = 1$ represents flat regions. We assume that the background light regions should satisfy high brightness and flat. Thus, the intersections of $Y_b = 1$ and $G_b = 1$ are selected as the candidates of background light regions. We dilation the intersections, and then select the connected regions among intersections which are greater than 5% size of the image as the background light regions.

To avoid the effects of suspended particles, we pick up the top 0.1% brightest pixels in the background light regions as the candidates of global background light. According to the characteristic of underwater optical imaging, the red light usually travels the shortest in water, which leads to the tone of underwater images dominated by bluish or greenish coloration. Therefore, the positions of global background light are related to the tone of input image. Firstly, we decide the dominant tone of input image as follows:

$$\begin{cases} I^B_{mean} > I^G_{mean} & \textit{Bluish tone} \\ I^B_{mean} \leq I^G_{mean} & \textit{Greenish tone}. \end{cases} \tag{10}$$

where I^B_{mean} and I^G_{mean} are the average values of blue channel and green channel (RGB color space). For the image with bluish tone, among the above-selected brightest pixels location, the RGB vector with the maximum blue-red difference in the input image is regarded as the global background light. Similarly, for the image with greenish tone, among the above-selected brightest pixels location, the RGB vector with the maximum green-red difference in the input image is regarded as the global background light. Such a selection trick guarantees the robustness of global background light estimation algorithm.

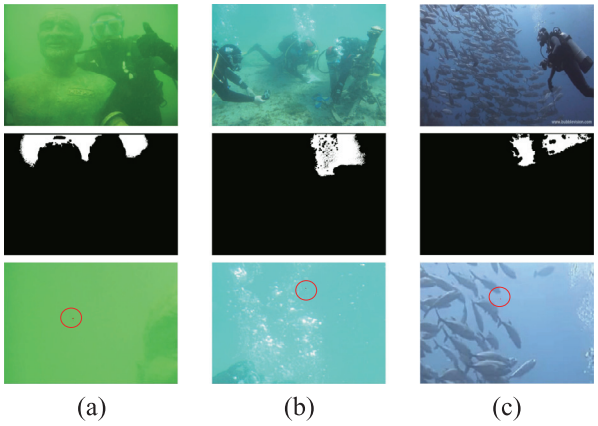

Fig. 3. Estimated global background light. (a) Example 1 (greenish underwater image). (b) Example 2 (bluish underwater image). (c) Example 3 (bluish underwater image). From top to bottom are raw underwater images, background light regions (white regions), and estimated global background light (red pixels in the red circles). (For interpretation of the references to colour in this figure legend, the reader is referred to the web version of this article.)

However, in some special cases, we might not find the candidates of background light regions, such as the underwater image without background. In such case, we assume the global background light $A^c = 1$. To show the effectiveness and robustness, Fig. 3 presents several examples of estimated global background light for underwater images with different tone.

4.3. Learning medium transmission

Learning-based strategies generally benefit from big data training [21]. Compared to the common image processing area, there is no easy way to have a degraded underwater image with reference image. Inspired by the idea of synthesizing samples [4,29], we attempt to simulate the blurring effect (light scattering) of underwater images to synthesize training samples. Because the blurring effect is similar with hazy, we use hazy image formation model [14] to synthesize the effect, and then generate our training samples. Specifically, given an image J^c_n, the global background light A^c and a random medium transmission $t^c \in [0, 1]$, the synthesized image I^c_w, which suffers from the effects of blurring by light scattering, can be described as:

$$I^c_w = t^c \cdot J^c_n + (1 - t^c) \cdot A^c, c \in \{r, g, b\}, \tag{11}$$

We use hazy image formation model to build our training samples because each channel of an image in hazy image formation model has the same global background light and medium transmission, which reduces the uncertainty of variables in the learning processing. Thus, we assume $A^c = 1$ and $t^r = t^g = t^b$. Moreover, ten random t^c are used for one image. Some synthesized results are shown in Fig. 4.

Next, we need to find some features which can represent the medium transmission. Dark channel feature, local max contrast feature, local max saturation feature, and hue disparity feature are related to the medium transmission [29]. The multi-scale dark channel features are defined as:

$$D_r = \min_{y \in \Omega_r(x)} \min_{c \in \{r,g,b\}} I^c(y)/A^c, \tag{12}$$

where $\Omega_r(x)$ is the image patch with size $r \times r$ centered at x. r represents the multi-scale. I^c is the input image. A^c is the global background light.

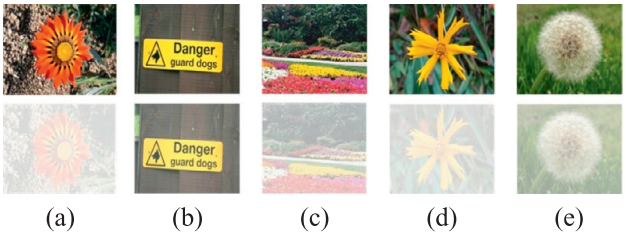

Fig. 4. Input images and the synthesized images. (a) t^c=0.15325. (b) t^c=0.81311. (c) t^c=0.41717. (d) t^c=0.18142. (e) t^c=0.15325.

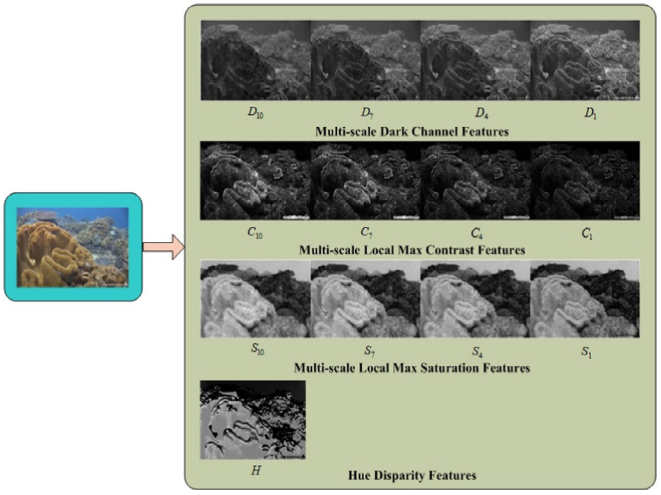

Fig. 5. Features related to the medium transmission.

The local contrast is defined as the variance of pixel intensities in a local image patch with size $r \times r$ compared to the center pixel value. The multi-scale local max contrast in a $s \times s$ region is described as:

$$C_r = \max_{y \in \Omega_r(x)} \sqrt{\frac{1}{3|\Omega_s(y)|} \sum_{z \in \Omega_s(y)} \|I(z) - I(y)\|^2}, \tag{13}$$

where $|\Omega_s(y)|$ is the cardinality of the local neighborhood $\Omega_s(y)$. s is fixed to 5 and r represents the multi-scale. I is the input image.

Following the definition of image contrast, the local max saturation is defined as the maximum of pixel-wise saturation values in a local image patch with size $r \times r$:

$$S_r = \max_{y \in \Omega_r(x)} \left(1 - \frac{\min_{c \in \{r,g,b\}} I^c(y)}{\max_{c \in \{r,g,b\}} I^c(y)}\right). \tag{14}$$

The hue disparity feature is defined as the hue disparity between the input image and its semi-inverse image:

$$H(I) = |I^h_{si} - I^h|, \tag{15}$$

where I_{si} represents the semi-inverse image, which means the maximum of input image and its inverse. I^h_{si} can be obtained by translating the semi-inverse image to the Lch color space, and then selecting the hue channel. Besides, I^h is the hue channel of the input image. In this letter, four scales (10, 7, 4, 1) are used for the dark channel feature, local max contrast feature and local max saturation feature. The features related to the medium transmission are shown in Fig. 5.

In the training stage, we extract the above-mentioned features from the synthesized images. For each feature map, 10 feature patches with size 5 × 5 are randomly sampled for making the medium transmission independent of the image content. We synthesize 1000 image samples, and then obtain 1000 × 13 feature maps, final extract 1000 × 13 × 10 feature patches. For one training sample, the extracted feature patches and one known medium transmission value are put into the random forest regression model [5].

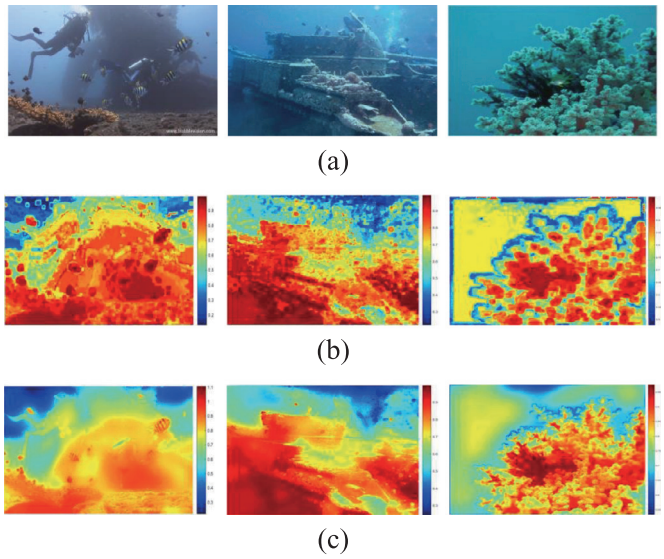

Fig. 6. Medium transmission. (a) Raw underwater images. (b) Coarse medium transmission. (c) Refined medium transmission. In the medium transmission, the color bar represents the different pixel values. (For interpretation of the references to colour in this figure legend, the reader is referred to the web version of this article.)

In the testing stage, the color corrected image is extracted the above-mentioned features. After that, the obtained feature maps are divided into 5 × 5 feature patches. After putting the feature patches from the same location into the trained model, a medium transmission value for the image patch located in the input image is obtained. The medium transmission value for each image patch of the input image is obtained by this way. To suppress the blocking artifacts of the patch-based medium transmission, the guided filter [15] is applied. The guide image is the blue channel of input underwater image. The size of filter is 41 × 41. The estimated medium transmission is shown in Fig. 6.

As shown in Fig. 6, the blocking artifacts are successfully reduced by the guided filter. Furthermore, the relative distances between the scene and the camera are well estimated. However, further experiments found that the assumption that three color channel of an underwater image have the identical medium transmission value does not always hold in the underwater scenario because different color light attenuates at different rates in water medium. In general, the red color channel is attenuated at a much higher rate than the blue and green color channels [8]. To thoroughly restore the visibility of the degraded underwater image, we assume that the estimated medium transmission belongs to red color channel. The medium transmission maps of the green and blue channels are estimated by exploring the correlation between the medium transmission and optical properties of underwater imaging.

4.4. Extending medium transmission to three channels

The total background light from the scene point to the camera can be obtained by integrating the attenuation from distance l=0 to l=d and casting up all scattering components at all directions [27]. The total background light can be expressed as:

$$B^c(d) = \int_0^d \int_\theta \beta^c(\varphi) E_a \exp(-p^c l) k_l \, \mathrm{d}l \, \mathrm{d}\varphi \tag{16}$$

where $B^c(d)$ is the total background light of the path-length d from the scene point to the camera, θ denotes all possible scattering angles for a certain scattering volume, $\beta^c(\theta)$ is the volume scattering function, E_a is the intensity of the ambient light and simplified to a constant, p^c is the total attenuation coefficient, k_l represents the properties of camera system and is a constant within a single image. Besides, $B^c(d)$ also can be described as:

$$B^c(d) = B^c(\infty)[1 - \exp(-p^c d)], \tag{17}$$

where $B^c(\infty)$ (i.e., A^c in Eq. (5)) is the global background light, and can is expressed as:

$$B^c(\infty) = \frac{k_l E_a}{p^c} \int_\theta \beta^c(\varphi)\, \mathrm{d}\varphi, \tag{18}$$

$\int_\theta \beta^c(\varphi)\mathrm{d}\varphi$ denotes scattering events toward the camera from all directions, and is essentially identical with the definition of scattering coefficient b^c in (7). $B^c(\infty)$ is rewritten as:

$$B^c(\infty) \propto \frac{b^c}{p^c}, c \in \{r, g, b\}. \tag{19}$$

Besides, Gould et al. found that scattering coefficient has an approximate linear relationship with light wavelength in general water [13], and is expressed as:

$$b^c = (-0.00113\lambda_c + 1.62517) b(\lambda_c), \tag{20}$$

where λ_r, λ_r, and λ_b are 620nm, 540nm, and 450nm in general water, respectively. $b(\lambda_c)$ can be simplified to the identical value in different color channels. According to (18) and (19), ratios of the total attenuation coefficient can be expressed as:

$$\frac{p^c}{p^r} = \frac{b^c B^r(\infty)}{b^r B^c(\infty)} = \frac{b^c A^r}{b^r A^c}, c \in \{g, b\}, \tag{21}$$

where p^g/p^r and p^b/p^r are the green-red total attenuation coefficient ratio and blue-red total attenuation coefficient ratio, respectively. According to (6), the medium transmission has an exponential correlation with the total attenuation coefficient. Therefore, the medium transmission of the green and blue channels is expressed as:

$$t^c(x) = (t^r(x))^{\frac{p^c}{p^r}}, c \in \{g, b\}. \tag{22}$$

The medium transmission of the green and blue color channels is not displayed because the differences among the medium transmission of different color channels are too minor to distinguish in the form of image.

Finally, with the estimated global background light and medium transmission of three channels, degraded underwater image is restored according to (5).

5. Experiment results

Our proposed method is compared with several state-of-the-art image enhancement and restoration methods: classical Dark Channel Prior method (DCP) [14], Retinex-based enhancement method (RBE) [10], and Red-channel method (RC) [11]. RC method and our proposed method are the variants of the classical DCP method. Thus, our method is compared with DCP method and RC method. In addition, our color correction algorithm is the same with the color correction algorithm proposed in RBE method. Consequently, it is obligatory to compare RBE method with our method. To verify the performance of different methods, subjective and objective evaluations are carried out, respectively. In order to evaluate the proposed method and help the development of underwater image enhancement and restoration research area, we collected an underwater image dataset from the Internet which includes 45 degraded underwater images. Raw underwater images presented in this letter are extracted from this collected dataset. The full dataset can be downloaded from https://www.dropbox.com/s/9qr0g544y67yi4b/underwater%20image%20dataset.rar?dl=0

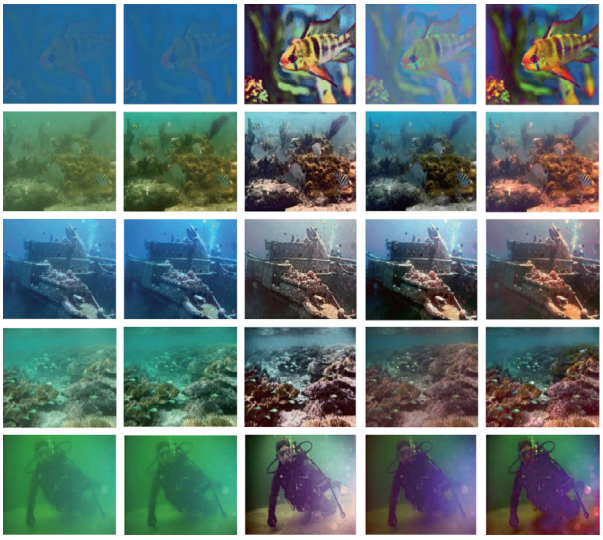

Fig. 7. Subjective performance comparison. (a) Raw underwater images. (b) DCP method. (c) RBE method. (d) RC method. (e) Our method.

5.1. Subjective performance comparison

As shown in Fig. 7, our method significantly unveils color and improves visibility of raw underwater images. Besides, our method restores most scene details and maintains natural appearance. DCP method has little effect on raw underwater images due to ignoring the fact that color of underwater image selective attenuation. Moreover, DCP method processes the three color channels of underwater image by the same medium transmission, which leads to unpleasing results. RBE method effectively increases the contrast and unveils the color of raw underwater images. However, there are over-enhanced areas in the results of RBE method due to ignoring the underwater imaging formation model. Additionally, RBE method is more prone to increasing noise and introducing artifacts. RC method improves the contrast and color of raw underwater images, and also produces relatively natural results. Compared with our method, RC method can not well restore the color and brightness.

5.2. Objective performance comparison

Image quality assessment (IQM) metric [2] is widely used for assessing the contrast change of the images captured in bad visibility scenes. We compared the contrast change of the results shown in Fig. 7. As shown in Fig. 8, the most predominant contrast change of our result is the amplification of the invisible contrast (blue). DCP method has little effect on the contrast. RBE and RC methods can amplify the invisible contrast (blue), but they produce much reverse of the contrast (red). The larger the loss (green) and reverse (red) of visible contrast are, the fewer details are unveiled.

To quantify the performance of different methods, underwater color image quality evaluation (UCIQE) metric [32] which is a comprehensive metric for evaluating chroma, saturation, and contrast of underwater image, and colorfulness measure (UICM) metric [31] which is new metric for testing the colorfulness of underwater image are employed. We compute UCIQE and UICM values of the above-mentioned methods on 30 underwater images which are randomly selected from our collected underwater image dataset. Besides, to demonstrate the effectiveness of our learning-based medium transmission estimation algorithm, we replace our medium transmission estimation algorithm with the

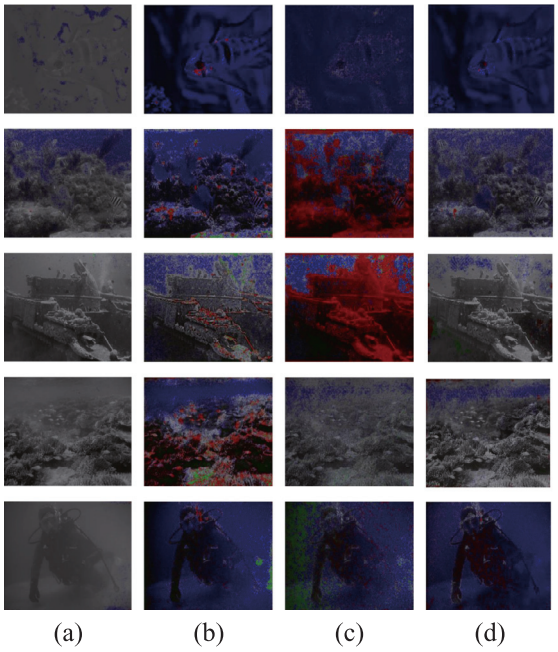

Fig. 8. Contrast change comparison. (a) DCP method. (b) REB method. (c) RC method. (d) Our method. In the contrast change image, green indicates that the contrast becomes invisible in the resulting image, blue indicates that the contrast becomes visible in the resulting image, red indicates that the contrast has different polarity between the result and the original image. (For interpretation of the references to colour in this figure legend, the reader is referred to the web version of this article.)

Table 1
Quantitative results in terms of UCIQE and UICM metrics.

Metric	DCP	REB	RC	CRC	Our
UCIQE	0.5125	0.5893	0.4896	0.5578	**0.6073**
UICM	3.8480	5.3340	3.9008	5.4496	**7.4959**

medium transmission estimation algorithm of RC, namely color correction + RC (CRC). Table 1 summarizes the average values of different methods in terms of UCIQE and UICM metrics. The values in bold indicate the best values.

As shown in Table 1, our results achieve the best values in terms of UCIQE and UICM metrics. The higher UCIQE value demonstrates that our results have better balance among the chroma, saturation, and contrast than the compared results. The higher UICM value indicates that our method better improves the color of underwater images. The standard deviation values for the scores of UICQE and UICM are 0.0498 and 1.4889, respectively. Additionally, compared with CRC method, the performance of our method is better than CRC method, which benefits from the learning-based strategy. Furthermore, we remove the underwater image dehazing method from our framework, the results of UCIQE and UICM are 0.5342 and 5.8619, which also demonstrates the effectiveness of our hybrid underwater image correction method.

6. Conclusion

This letter has presented a hybrid method for underwater image correction. In addition, an underwater image dataset is collected. Subjective evaluation shows that our method improves the contrast and brightness, restores color, and produces natural appearance. Objective evaluation demonstrates that the proposed method achieves the best results in terms of two latest underwater image quality evaluation metrics when compared with several existing methods.

Acknowledgments

This work was supported in part by the National Key Basic Research Program of China (2014CB340403) and the Natural Science Foundation of Tianjin (15JCYBJC15500). The authors would like to thank Yang, M. for providing the code of the UCIQE metric, and the foundational works of [14] and [29].

References

[1] C. Ancuti, C.O. Ancuti, Enhancing underwater images and videos by fusion, in: IEEE Int. Conf. Comput. Vis. Pattern Recognit. (CVPR) (2012) 81–88.
[2] T.O. Aydin, R. Mantiuk, K. Myszkowski, H.S. Seidel, Dynamic range independent image quality assessment, in: Proc. SIGGRAPH (2008) 1–10.
[3] G. Bianco, M. Muzzupappa, F. Bruno, R. Garcia, L. Neumann, A new color correction method for underwater imaging, Int. Arch. Photogramm. Remote Sens. Spatial Inf. Sci. 40 (2015) 25–32.
[4] M. Boffety, F. Galland, A.G. Allais, Color image simulation for underwater optics, Appl. Opt. 51 (2012) 5633–5642.
[5] L. Breiman, Random forests, Mach. Learn. 45 (2001) 5–32.
[6] N. Carlevaris Bianco, A. Mohan, R.M. Eustice, Initial results in underwater single image dehazing, in: IEEE Int. Conf. OCEANS (2010) 1–8.
[7] J.Y. Chiang, Y.C. Chen, Underwater image enhancement by wavelength compensation and dehazing, IEEE Trans. Image Process. 21 (2012) 1756–1769.
[8] P. Drews, E. Nascimento, F. Moraes, Transmission estimation in underwater single images, in: IEEE Int. Conf. Comput. Vision (ICCV) (2013) 825–830.
[9] P.L. Drews, E.R. Nascimento, S.S. Botelho, M.F. Campos, Underwater depth estimation and image restoration based on single images, IEEE J. Comput. Graph. Appl. 36 (2016) 24–35.
[10] X. Fu, P. Zhuang, Y. Huang, Y. Liao, X.P. Zhang, X. Ding, A retinex-based enhancing approach for single underwater image, in: IEEE Int. Conf. Image Process. (ICIP) (2014) 4572–4576.
[11] A. Galdran, D. Pardo, A. Picon, A. Alvarez Gila, Automatic red-channel underwater image restoration, J. Vis. Commun. Image Rep. 26 (2015) 132–145.
[12] A.S.A. Ghani, N.A.M. Isa, Underwater image quality enhancement through integrated color model with rayleigh distribution, Appl. Comput. 27 (2015) 219–230.
[13] R. Gould, R. Arnone, P. Martinolich, pectral dependence of the scattering coefficient in case 1 and case 2 waters, Appl. Opt. 38 (1999) 2377–2383.
[14] K. He, J. Sun, X. Tang, Single image haze removal using dark channel prior, IEEE Trans. Pattern Anal. Mach. Intell. 33 (2011) 2341–2353.
[15] K. He, J. Sun, X. Tang, Guided image filtering, IEEE Trans. Pattern Anal. Mach. Intell. 35 (2013) 1397–1409.
[16] B. Henke, M. Vahl, Z. Zhou, Removing color cast of underwater images through non-constant color constancy hypothesis, in: IEEE Int. Symp. Image Signal Process. Anal. (ISPA) (2013) 20–24.
[17] K. Iqbal, S.R. Abdul, M. Osman, A.Z. Talib, Underwater image enhancement using an integrated colour model, IAENG Int. J. Comput. Sci. 32 (2007) 239–244.
[18] K. Iqbal, M. Odetayo, A. James, Enhancing the low quality images using unsupervised colour correction method, in: IEEE Int. Conf. Syst. Man Cybern. (2010) 1703–1709.
[19] J.S. Jaffe, Computer modeling and the design of optimal underwater imaging systems, IEEE J. Ocean. Eng. 15 (1990) 101–111.
[20] K. Lebart, C. Smith, E. Trucco, D.M. Lane, Automatic indexing of underwater survey video: algorithm and benchmarking method, IEEE J. Ocean. Eng. 28 (2003) 673–686.
[21] Y. LeCun, Y. Bengio, G. Hinton, Deep learning, Nature 521 (2015) 436–444.
[22] C. Li, J. Guo, Underwater image enhancement by dehazing and color correction, J. Electr. Imaging 24 (2015) 033023.
[23] H. Liu, P. Chau, Underwater image color correction based on surface reflectance statistics, in: Proc. IEEE Asia Pacific Signal Inf. Process. Assoc. (APSIPA) (2015) 996–999.
[24] B.L. McGlamery, A computer model for underwater camera systems, in: Proc. SPIE Ocean Opt. VI (1980) 221–231.
[25] Y.T. Peng, X. Zhao, P.C. Cosman, Single underwater image enhancement using depth estimation based on blurriness, in: IEEE Int. Conf. Image Process. (ICIP) (2015) 4952–4956.
[26] Y. Schechner, N. Karpel, Clear underwater vision, in: IEEE Int. Conf. Comput. Vision Pattern Recognit. (CVPR) (2004) 536–543.
[27] Y. Schechner, Y. Yoav, N. Karpel, Clear underwater vision, in: IEEE Int. Conf. Comput. Vision Pattern Recognit. (CVPR) (2004) 536–543.
[28] N.J.C. Strachan, Recognition of fish species by colour and shape, J. Image Vis. Comput. 11 (1993) 2–10.
[29] K. Tang, J. Yang, J. Wang, Investigating haze-relevant features in a learning framework for image dehazing, in: IEEE Int. Conf. Comput. Vision and Pattern Recognit. (CVPR) (2014) 2995–3002.
[30] E. Trucco, A.T. Olmos Antillon, Self-tuning underwater image restoration, IEEE J. Ocean. Eng. 31 (2006) 511–519.
[31] K. Yang, C. Gao, S. Agaian, Human-visual-system-inspired underwater image quality measures, IEEE J. Ocean. Eng. pp (2015) 1–11.
[32] M. Yang, A. Sowmya, An underwater color image quality evaluation metric, IEEE Trans. on Image Process. 21 (2015) 1215–1219.